Chapter 3

Synthesis of curcumin conjugated gold nanoparticles and their in-vitro antibacterial and cellular responses

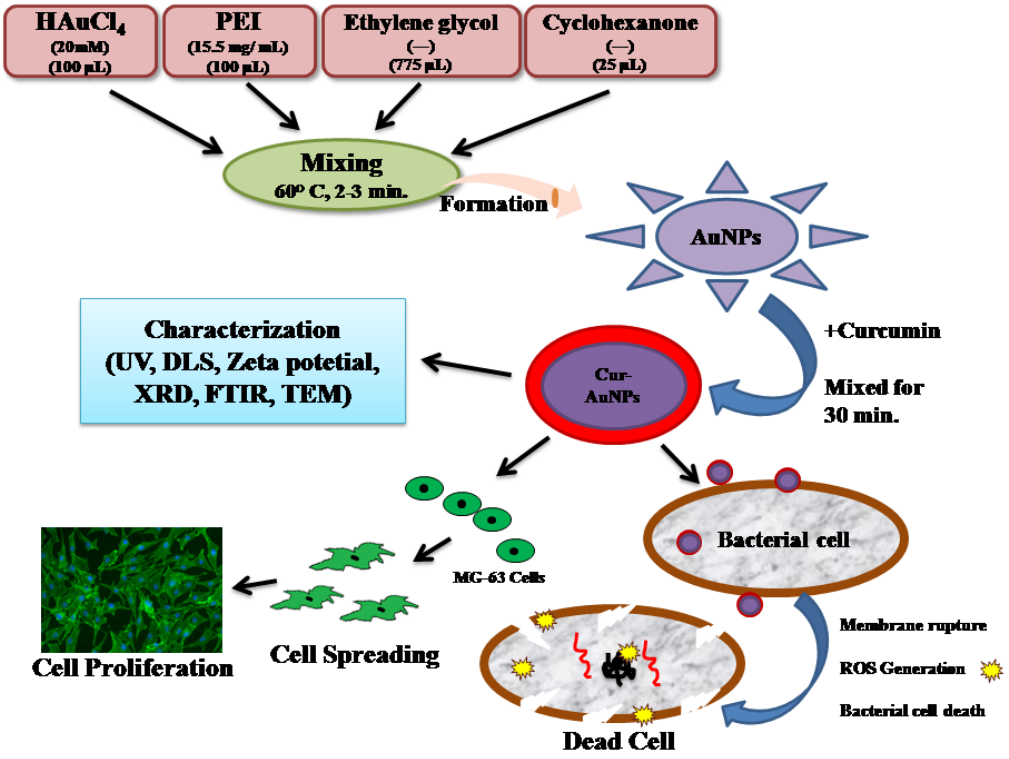

3.1 Introduction

Due to the rise and dissemination of drug resistance among bacterial infections, antibiotics usually lose their efficiency over time. All these "antibiotic resistance crisis" and iatrogenic disorders triggered by drug-resistant bacteria results in additional billions of dollars in annual medical costs (Rossolini et al., 2014; Zhao et al., 2011; Li et al

2014). In light of this grave scenario, it is crucial to explore for better approaches to combat them.

Nanoparticles provide a universal platform for therapeutic applications and fight microorganisms that are resistant to conventional antibiotics owing to their distinctive chemical and physical properties (Li et al 2014 and Chu et al., 2018). Because of their malleable size, shape, surface properties, tuneability, optical properties, biocompatibility, minimal cytotoxicity, high stability, and potential for various functionalities, gold nanoparticles are promising candidate for inclusion in a number of medical applications (Ashraf et al., 2016). Natural yellow secondary metabolite Cur, which comes from the *Curcuma longa* plant, has been shown to have anti-inflammatory, antioxidant, and antibacterial properties (Lee et al., 2013; Chattopadhyay et al., 2004; Senft et al., 2010). This rhizome has a variety of medical uses, including the treatment of burns, heated swellings, small pox, mouth and stomach ulcers (Al Kashmiri et al., 2010; Khanna et al., 1999; Nadkami et al., 1976). While curcumin has medical potential, its low aqueous solubility and low bioavailability severely restrict its use, raising substantial safety concerns. Several methods have been used to increase the bioavailability of curcumin. Some of these methods involved loading curcumin into micelles and encapsulating curcumin in liposomes (Agashe et al., 2011; Mohanty et al., 2010; Mohanty et al, 2012). Curcumin-encapsulated liposome research could be impeded in the future by poor storage stability, rapid leakage of water-soluble drugs in the presence of blood components, and low encapsulation efficiency. Furthermore, complicated micelle loading techniques and drug loading should also be addressed. To enhance the molecule's bioavailability, functionalizing it by conjugating it with a hydrophilic molecule has also been explored (Yadav et al., 2020). The therapeutically active group of the molecule is hindered by this process, jeopardising the primary objective of conjugation.

Bonding curcumin to gold or other noble metal nanoparticles is an alternative technique. Curcumin's activity, particularly in aqueous conditions, its half-life, overall stability, in both proprietary and non-proprietary metabolic pathways can all be improved by conjugating curcumin to nanoparticles (Sindhu et al., 2011). Recently, a variety of methods have been proposed in this area to investigate the diverse applications of curcumin (Krishnakumar et al., 2010; Bhawana, Basniwal et al., 2011; Yallapu et al., 2012). Since, AuNPs make a promising choice for antibiotic complementation because their antibacterial function has become a recent focus of intense research. Through the formation of holes in the bacterial cell wall, AuNPs antibacterial activity kills bacteria by preventing the loss of their internal organelles, which leads to cell death. In addition, by binding to bacterial DNA and inhibiting the uncoiling of DNA during transcription, AuNPs can suppress infections that are resistant to many drugs (Arafa et al., 2018). Recently, S. Manju et al. reported on the fabrication of water-soluble gold nanoparticles in a curcumin-polymer (hyaluronic acid) conjugate and examined it for blood compatibility and targeted drug administration onto malignant cells (Manju et al., 2012). However, Curcumin and hyaluronic acid were also conjugated, and the chloroauric acid was subsequently reduced to create gold nanoparticles in the solution. The major therapeutic group of this molecule gets involved in the conjugation, which decreases its availability for its therapeutic use to any biological system, despite the fact that bioavailability rises with conjugation, as demonstrated in this and many others published methods (Daniel et al., 2004). Therefore, further study is required that would not only increase the bioavailability of the molecule but also maintain its therapeutic effectiveness and give the conjugated system multifunctional features. There are numerous studies in favour of curcumin-functionalized, -coated, or -conjugated gold nanoparticles, but they all implicate the direct reduction of gold ions ($HAuCl_4$) using curcumin (without the use

of other reducing or reducing and stabilizing agent), which has the limitation of taking too much time, using a lot of reagents, and usually requires a long and tedious purification process to remove excess curcumin(Singh et al., 2013; Sindhu et al., 2014; Shaabani et al., 2017; Muniyappan et al., 2021; Nambiar et al., 2018; Sreelakshmi et al., 2013; Govindaraju et al., 2018). Therefore we proposed a simple electrostatic interaction method for conjugation of Cur on AuNPs surface without disturbing its therapeutic groups. For this we used previously synthesised AuNPs in our lab using PEI [**PC Pandey 2010 Indian Patent 343222]** (Pandey et al., 2016). It has been reported that polymer like polyethylenimine (PEI) plays a role in the regulated production of AuNPs under ambient settings, with the possibility of a selective interaction with DNA binding proteins (Pandey et al., 2017). It has already been reported that the cationic polymer PEI plays a key role in both the quick reduction of gold cations into gold nanoparticles and the production of cationic coating for drug loading (Pandey et al., 2016). PEI plays a multifunctional role, such as providing a positive charge, controlling the size, and stabilising the nanoparticles (Do et al., 2014; Jia et al., 2016; Mohammed et al., 2013). PEI has a significant number of primary amino groups which enable PEI to be used as a stabilising agent to form various nanoparticles, including metal and metal oxide nanoparticles (Do et al., 2014; Wen et al., 2013; Lee et al., 2011). In addition, it also controls the maturation of gold nanoparticles by protecting the gold nanoparticles surface (Mohammed et al., 2013).

This chapter demonstrates the synthesis of highly stable, water-dispersible Cur-AuNPs and its evaluation as potential antibacterial and antibiofilm agent along with *in vitro* cytotoxicity studies. Cur-AuNPs were conjugated using an electrostatic interaction between positively charged polyethylenimine (PEI)-capped AuNPs and negatively charged curcumin's outer surfaces. UV-Vis spectrometry is used to monitor the nano-

synthesis process. The crystalline, coated compounds, size, shape, and elemental compositions of the synthesised conjugated nanoparticles are characterized by XRD, FTIR, TEM, DLS, and Zeta potential. In this chapter, the advance and unambiguous synthesis process of AuNPs and curcumin conjugated AuNPs with significant stability (up to 6-7 months at room temperature) has been demonstrated. The mechanism of evolution of crystalline and spherical Cur-AuNPs is elucidated using HRTEM and absorbance spectroscopy which indicate stable conformation of curcumin on the AuNPs. In addition, the chapter also demonstrates the consequences of Cur-AuNPs on antibacterial and cellular response of conjugated nanoparticles.

3.2 RESULTS AND DISCUSSION

Our research focuses on identifying the long-standing issue of why curcumin cannot be used as a first-line therapeutic agent due to its instability and water insolubility. The synthesis of highly water-dispersible curcumin and the subsequent assessment of its synergistic effects against an isolate of *Klebsiella pneumoniae* (MDR bacteria) have been demonstrated in subsequent sections.

3.2.1 UV-Vis absorbance Spectroscopy

Figure 3.1 (a) shows the typical spectra of Curcumin, AuNPs and Cur-AuNPs. The UV spectrum of Curcumin and AuNPs showed the absorption maximum at ~420 and ~520 nm respectively. In the case of Cur-AuNPs, the absorption measurements indicated that the plasma resonance wavelength λ max at ~535 nm with a small peak at ~420 nm. The shift in peak from 520 to 535 nm shows the coupling between AuNPs and Cur. The spectra of Cur-AuNPs have been taken at different time intervals (15 min, 30 min, 60 min, and 120 min, overnight and after 6 months) and shown with comparison to AuNPs spectra (Figure 3.1b).

The analysis showed that the surface plasmons absorbance band of Cur-AuNPs remained centered at ~535 nm after 6 months with little decrease in its absorbance without any shift in its wavelength which shows the stability of the Cur-AuNPs at room temperature. The red shift observed in this study for the spectrum of Cur-AuNPs was related to the changes in their surface due to modification with curcumin (Gangwar et al., 2012).

The strong band of AuNPs absorption observed at approximately 520 nm was attributed to the collective oscillations of electrons on the surface of gold nanoparticles called plasmon resonance. Furthermore, the small band at approximately 400 nm in the spectrum of Cur-AuNPs corresponded to the characteristic absorption band of curcumin, indicating conjugation (Campos et al., 2017). Furthermore, no change was observed in the spectra at 400 nm.

3.2.2 Dynamic Light Scattering (DLS) and Zeta potential

Figure 3.2 shows the DLS and Zeta potential analysis of AuNPs and Cur-AuNPs. The hydrodynamic size of Cur-AuNPs [60.38 nm, Figure 3.2(d)] was larger than AuNPs [41.2 nm, Figure 3.2 (b)] because of presence of curcumin on the surface of gold nanoparticles. Zeta potential values for both systems presented a highly positive/negative surface charge, 42 mV [Figure 3.2(a)] and -32 mV [Figure 3.2(c)] in the AuNPs and Cur-AuNPs suspension, respectively, which indicated electrostatic stability.

After conjugating with curcumin, AuNPs surface charge reduced, implying that curcumin was capable of altering the surface nature. According to studies, electrostatically stabilised particles must have a zeta potential of at least 30 mV in order to generate a physically stable nanosuspension (Gao et al., 2010; Kamble et al., 2010).

Negative surface charge causes little aggregation and high stability with prolonged storage (Yallapu et al., 2012). Cur-AuNPs were found to be stable for a period of six

months. Throughout this period of storage, the spectroscopic features (colour, appearance, and so on) remained unaltered (Elbialy et al., 2019).

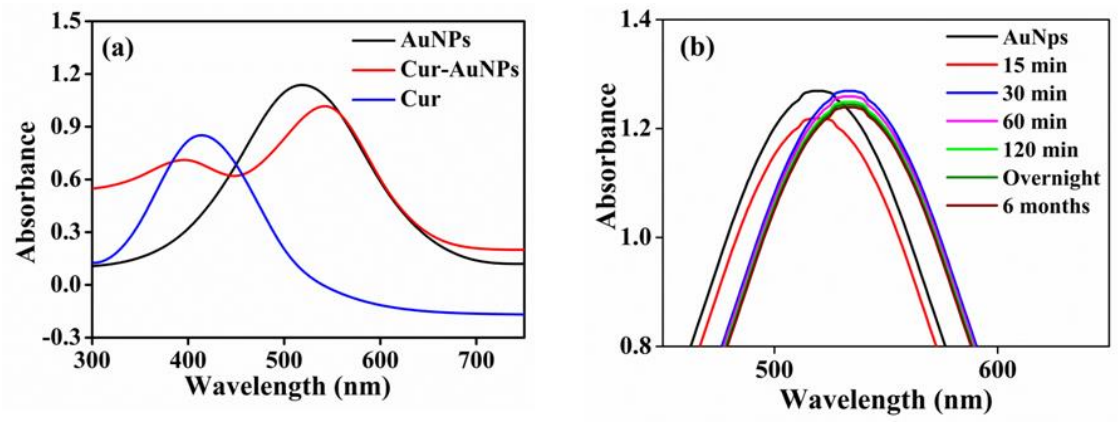

Figure 3.1 *Representing (a) UV-vis absorbance Spectrometry of Cur, AuNPs and Cur-AuNPs (b) absorbance spectra of Cur-AuNPs for different time interval compared with AuNPs spectra.*

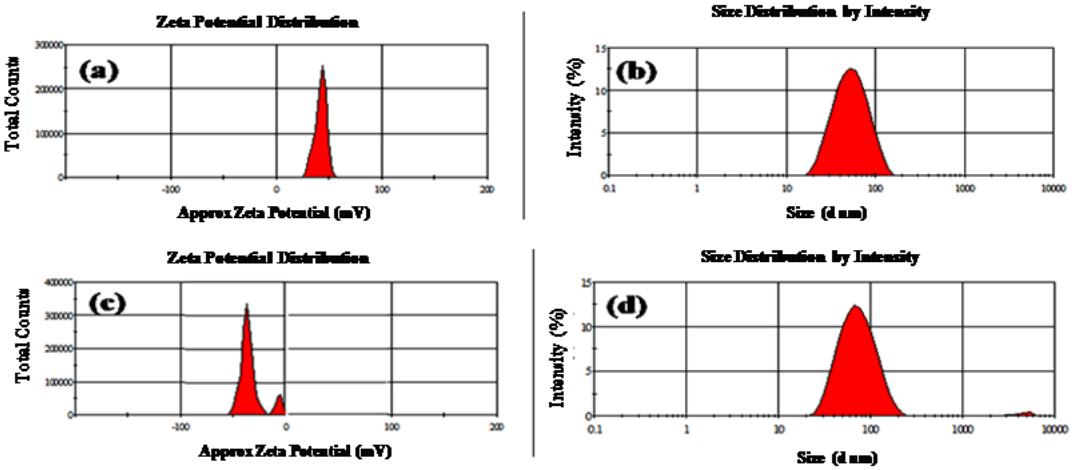

Figure 3.2 *Zeta potential of AuNPs (a) and cur-AuNPs (c) & their corresponding DLS (b) & (d) respectively.*

3.2.3 X – ray diffraction (XRD)

Figs. 3.3 (a, b and c) represent the X-Ray diffraction (XRD) patterns of AuNPs, Cur and Cur-AuNPs. The presence of four diffraction peaks at 38.26, 44.33, 64.53, and 77.67°

were observed in XRD of AuNPs. These peaks correspond to (111), (200), (220), and (311) sets of lattice planes that are indexed to face-centred cubic (fcc) crystal structure (JCPDS No. 04–0784) (Al Shehab et al., 2020). The appearance of these four intense peaks confirms the crystalline phase of AuNPs.

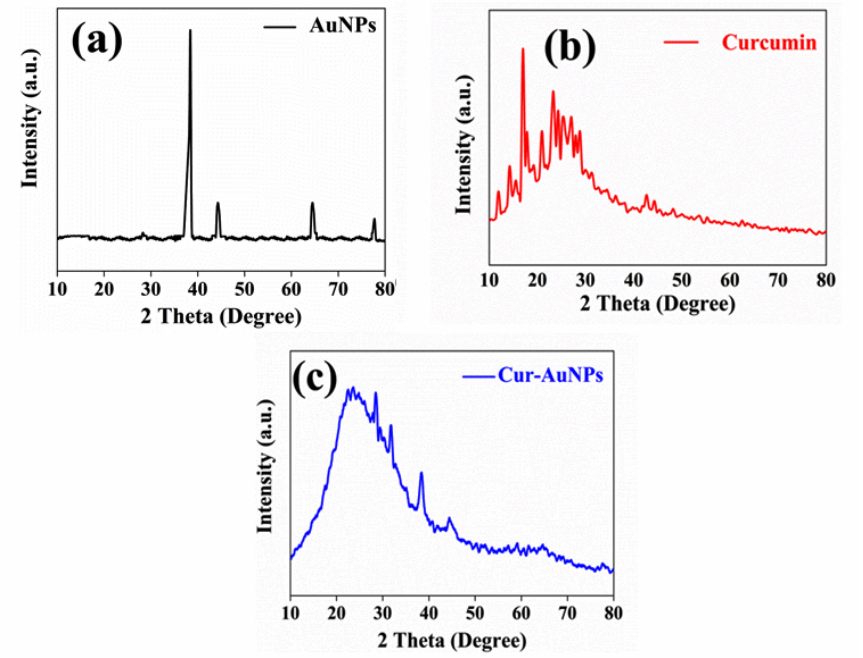

Figure 3.3 *X- Ray Diffraction (XRD) patterns of (a) AuNPs, (b) Curcumin and (c) Cur-AuNPs*

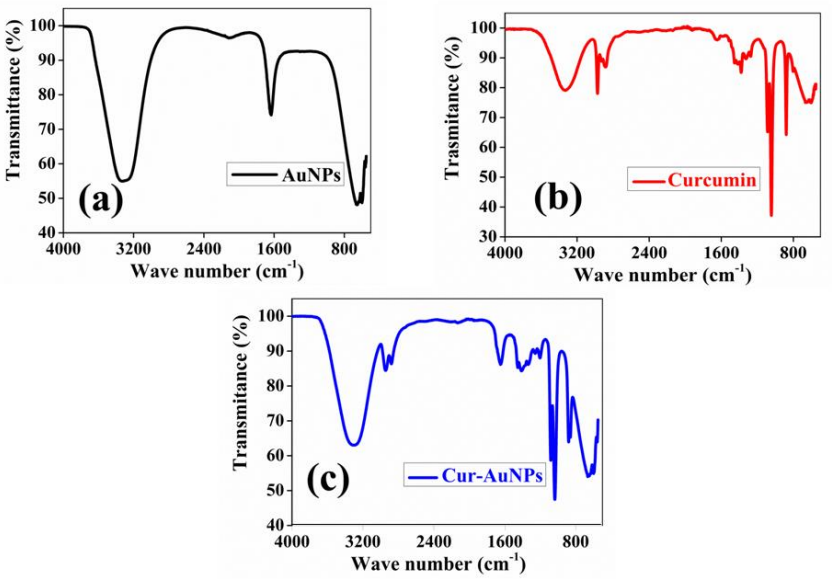

Figure 3.4 *FTIR spectra of (a) AuNPs, (b) Curcumin, (c) Cur-AuNPs.*

The nanoparticle size was calculated using Debye–Scherrer's Equation 3.1

$$\mathbf{Dp = 0.9\ \lambda / \beta\ cos\theta} \qquad \mathbf{(3.1)}$$

Dp is crystallite size; λ is wavelength of CuKα (1.54060 Å); θ is Bragg angle; β is full width at half maxima (FWHM). The average crystallite size of gold nanoparticles was found to be 17.47 nm.

3.2.4 Fourier transforms infrared spectroscopy (FTIR)

The FTIR spectra of AuNPs, Cur and Cur-AuNPs are shown in Figs. 3.4 (a, b, and c). Three distinct peaks were observed at about 3300 cm^{-1}, 1640 cm^{-1} and 690 cm^{-1} which represent the stretching vibrations caused by the hydroxyl group, C=C and C-C, respectively (Khademi-Azandehi et al., 2015). The stretching vibration of the curcumin ligand is seen in Figure 3.4(b) at 3200–3500 cm^{-1} due to O–H groups, while the stretching vibration of the C–C aromatic chain is shown at approximately 1427 cm^{-1} (Tsonko et al., 2005). In addition, a sizable intensity band at about 1110 cm^{-1} was linked to the C-O band's bending vibration. The FTIR of Cur-AuNPs is shown in Figure 3.4(c). It is evident that the primary peaks are not changing, indicating that the final Cur-AuNPs have not been dissociated.

3.2.5 Transmission Electron Microscopy (TEM) and Selected Area Electron Diffraction SEAD pattern

The morphology and size of AuNPs/Cur-AuNPs were evaluated using TEM. Particles size was calculated using image J software by measuring the diameter of approximately 50-60 nanoparticles and the statistical analysis was done on Origin. The TEM measurements and size distribution analysis of the AuNPs and Cur-AuNPs showed that particles are spherical in shape (Figs. 3.5a and 3.5d) with an average core diameter to be

around 10 and 13 nm respectively (Figs. 3.5b and 3.5e). The selected area electron diffraction (SAED) pattern generated from the AuNPs and Cur-AuNPs is displayed in Figs. 3.5c and 3.5f.

The surface conjugation of curcumin on AuNPs is further supported by the increase in size of Cur-AuNPs and then AuNPs. The distinct lattice fringes in the high resolution TEM pictures and the typical SAED pattern with bright circular rings corresponding to the (111), (200), (222), and (311) planes are confirmation of the produced nanoparticles' high degree of crystallinity. The population of AuNPs with a diameter of less than 10 nm has the maximum density, as shown in Figure 3.5.

3.2.6 Antibacterial studies

3.2.6.1 Minimum inhibitory concentration (MIC) determination and time dependent bacterial killing

MIC of Cur, AuNPs, Cur-AuNPs, against *Klebsiella pneumoniae* was determined by broth micro-dilution assay (Figure 3.6a). The MIC of curcumin (≥ 128 µg/ml) was found to be highest compared to AuNPs and Cur-AuNPs, which was consistent with the previous studies (Singh et al., 2017). Cur-AuNPs exhibited the highest efficiency i.e., lowest MIC (8 µg/ml) indicating that curcumin conjugated with AuNPs significantly enhanced its bactericidal potential. To check the time-dependent effect of MIC concentration of Cur, AuNPs, and Cur-AuNPs (i.e., 128 µg/ml, 32µg/ml and 8 µg/ml, respectively) on the growth of aforementioned resistant bacteria isolates was investigated in the microtiter plates by the $\log_{10}$ CFU/ml reduction. One can note the rarefaction of bacterial population with the increase in incubation time, almost complete lysis after 24 h exposure to Cur-AuNPs (Figure 3.6 b).

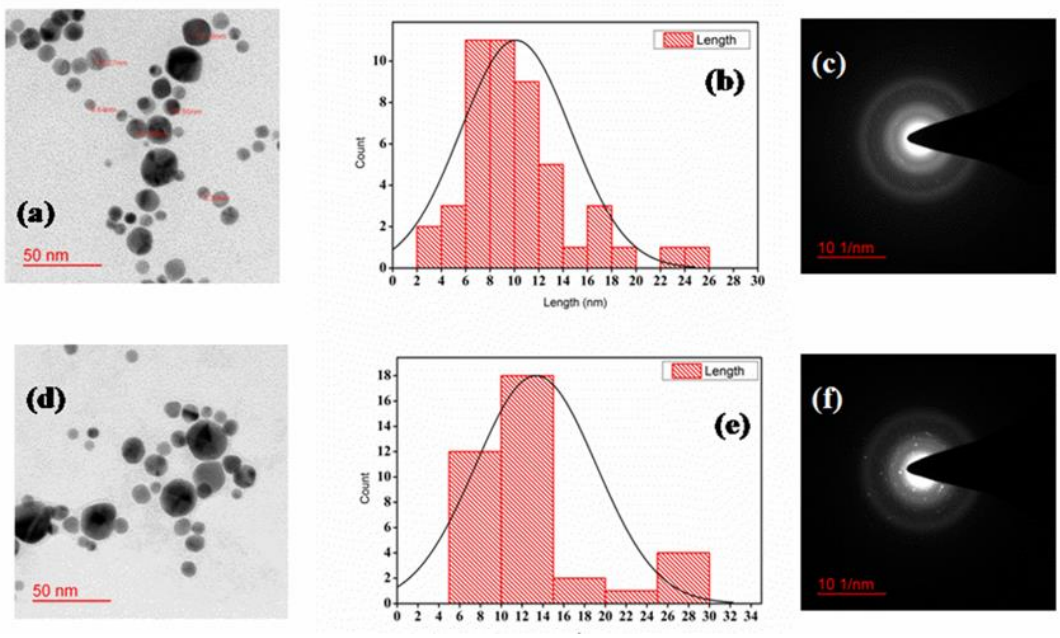

Figure 3.5 *TEM images of (a) AuNPs, (b) Particles size of AuNPs, (c) SAED pattern of AuNPs, (d) Cur-AuNPs, (e) Particles size of Cur-AuNPs, (f) SAED pattern of Cur-AuNPs.*

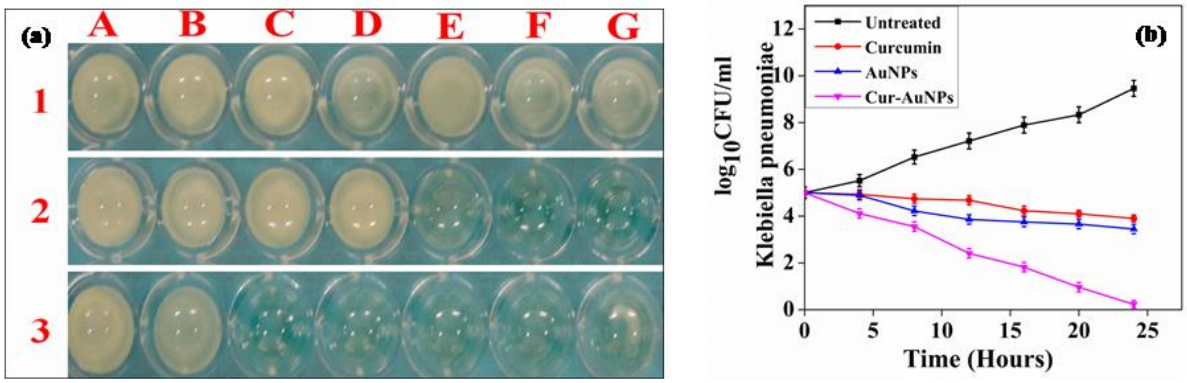

Figure 3.6 (a) *MIC determination by microbroth dilution method 1) Curcumin treated (≥128 µg/ml) 2) AuNPs treated (32 µg/ml) 3) Cur-AuNPs treated (8 µg/ml). Wells A-G contain serially doubly diluted test compounds ranging from 128 µg/ml (well G) to 2 µg/ml (well A)****; (b)*** *Kill curves for log-phase growing multi-drug resistant Klebsiella pneumoniae treated with MIC concentration of Cur (128 µg/ml), AuNPs (32 µg/ml), Cur-AuNPs (8 µg/ml)*

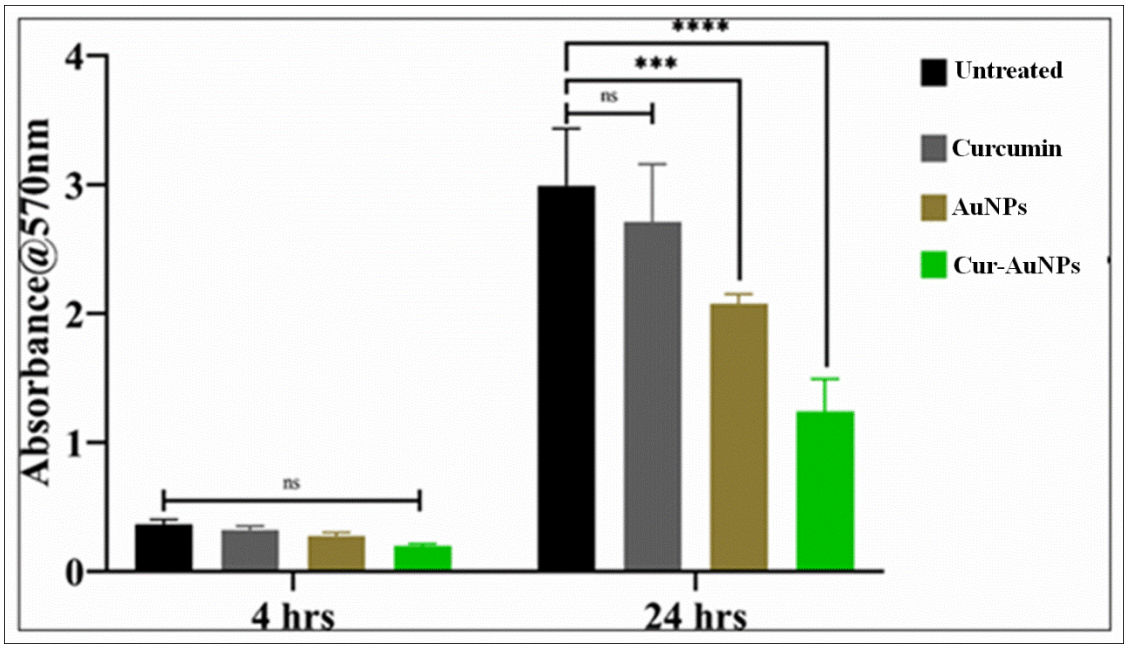

Figure 3.7 *Crystal violet based antibiofilm assay. Plot depicting absorbance readings with different test samples at 4 and 24 h.*

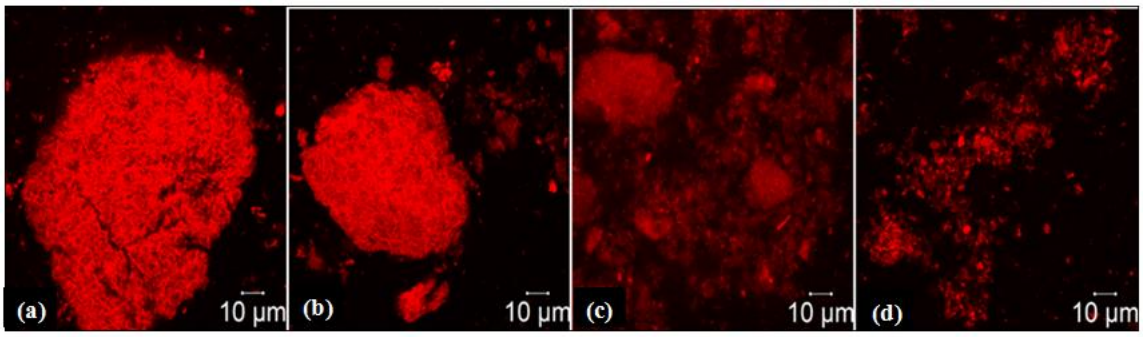

Figure 3.8 *Confocal micrographs of nanoparticle treated hvKP biofilms. (a) Confocal section of untreated biofilms of hvKP (b) Confocal section of curcumin (128 µg/ml) treated biofilm of hvKP (c) Confocal section of AuNPs (32 µg/ml) treated biofilm of hvKP (d) Confocal section of Cur-AuNPs (8 µg/ml) treated biofilm of hvKP.*

3.2.6.2 Antibiofilm activity determination

While observing the inhibitory effect of Cur, AuNPs, and Cur-AuNPs (conc.128 µg/ml, 32 µg/ml and 8 µg/ml, respectively) on antecedently formed biofilms, 54.2% inhibition was noted when treated with Cur-AuNPs; while individually curcumin and AuNPs were found to foster 8% and 24% of biofilm inhibition (Figure 3.7). At early time point, all the

test compounds had insignificant effect whereas, at late time point (24 h), Cur-AuNPs were found very effective. It was found better than both Cur and AuNPs used alone.

3.2.6.3 CLSM evaluation of the antibiofilm activity of Cur, AuNPs, Cur-AuNPs

After CV assay, we evaluated the disintegration of antecedently formed biofilm of hvKP by curcumin, AuNPs and Cur-AuNPs by employing confocal microscopy using the red fluorescent dye ConA-TR (Figure 3.8).

In agreement with the data obtained by phenotypic characterization by CV assay, biofilm of hvKP isolate showed an intense Con A-TR staining, indicating the presence of a marked amount of the sugars (Figure 3.8a). Seventy-two hours old biofilms hvKP isolate was imaged after addition of Cur, AuNPs and Cur-AuNPs at concentration 128 µg/ml, 32 µg/ml and 8 µg/ml, respectively. Compared to the untreated control, Cur-AuNPs arbitrated clear biofilm matrix disintegration as evident by the tiny red dots and reduced intensity of red fluorescence (Figs. 3.8a and 3.8d). AuNPs also triggered disintegration of matrix but curcumin had insignificant effect on the matrix (Figs. 3.8b and 3.8c).

3.2.6.4 Changes in membrane dynamics

The confocal microscopic studies have revealed the matrix disintegration and CFU log reduction assay unfolded the bactericidal activity of Cur, AuNPs and Cur-AuNPs; therefore; we looked into the mechanism. We investigated Cur-AuNPs mediated perturbations in membrane lipid dynamics by using DPH assay. DPH interacts with acylated lipids of the cell membrane, therefore intercalates in it, and hence fluoresce (Yadav et al. 2020). However, if the membrane integrity is compromised, insertion of DPH into the membrane does not take place, and hence its fluorescence is also forfeited. We assessed it using flow cytometry. Interestingly, Cur (128 µg/ml) induced a ~45%

right shift, indicating disturbed acyl groups (Figure 3.9B), while AuNPs (32 µg/ml) triggered a negligible right shifting (1%) of the population that indicates the negligible acyl shifting/ change in membrane dynamics (Figure 3.9C). However, the incorporation of Cur-AuNPs (8 µg/ml) led a ~65 % right shift, indicating increase in cell population (65.3%) that had taken up DPH designating significant alteration in membrane lipids or perturbed membrane acyl groups (Figure 3.9D). As we can see in Figure 3.9 (E), wherein, the untreated control exhibited negligible acyl shifting.

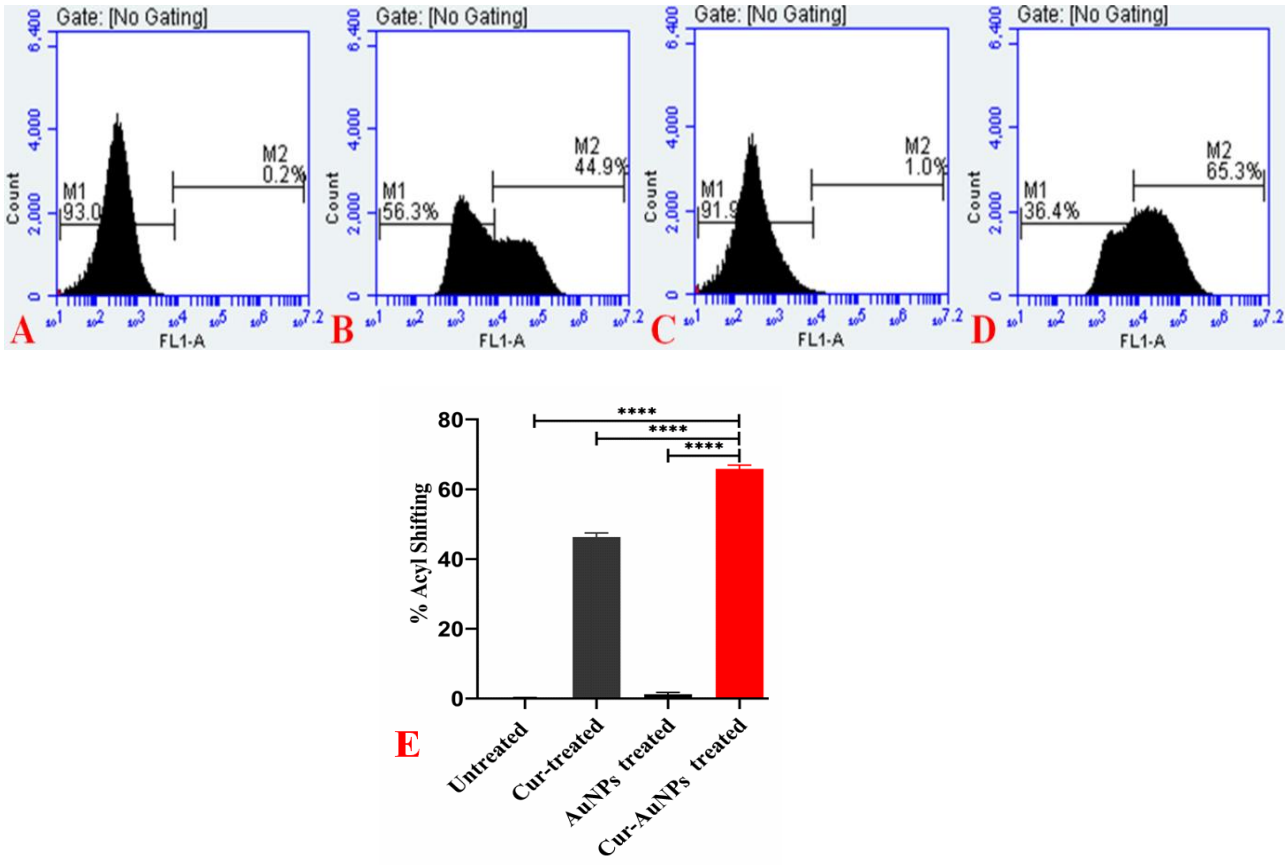

Figure 3.9 *Acyl shifting assay for membrane alteration (A) Untreated (B) Curcumin treated (128 µg/ml) (C) AuNPs treated (32 µg/ml) (D) Cur-AuNPs (8 µg/ml) treated. (Graph was generated and analyzed using GraphPad 8.0 (San Diego, CA) (E) Statistical analysis of acyl shifting population for untreated, Cur (128 µg/ml) treated, AuNPs (32 µg/ml) treated and Cur-AuNPs (8 µg/ml) treated*

The incubation of *Klebsiella pneumoniae* with MIC concentration of Cur-AuNPs showed significantly increases in acyl shifting in comparison to Cur and AuNPs alone. As depicted in Figure 3.9 (E), the acyl shifting was about ~45% and ~1% for Cur and AuNPs treated *K. pneumoniae.* However, upon treatment with Cur-AuNPs conjugate, the acyl shifting was found to be 65.3% that indicate significant alteration in membrane lipids. Thus, it can be concluded that the conjugation of curcumin on AuNPs rendered its enhanced potential to foster membrane acyl shift.

3.2.6.5 Reactive oxygen species generation

Results of membrane dynamics assay were very encouraging and then we evaluated ROS generation employing 2′, 7′-dichlorfluorescein-diacetate (DCFH-DA) through flow cytometry after treatment with curcumin, AuNPs, Cur-AuNPs (at concentration 128 µg/ml, 32 µg/ml and 8 µg/ml, respectively). We observed significant differences in the ROS generation profiles of these compounds (Figure 3.10A-D). Compared to the individually treated with curcumin and Au-NPs, the Cur-AuNPs induced a significant increase in the DCF fluorescence.

In Cur treated group only 38.3% cells exhibited the ROS generation while in the AuNPs treated group, the overall ROS generating population increased to 42.4% (Figure 3.10B, C).Interestingly, Cur-AuNPs treatment resulted in massive ROS generation; around 60.0% cells were found to generate ROS (Figure 3.10D). As we can see in Figure 3.10 (E), wherein, the untreated control cell population exhibited negligible ROS generation. The incubation of *Klebsiella pneumoniae* with MIC concentration of Cur-AuNPs showed significantly increases in ROS generating cell population in comparison to Cur and AuNPs treatment alone. As depicted in Figure 3.10 (E), the ROS generating cell population was about 38.3% and 42.4% for Cur and AuNPs treated *K. pneumoniae*.

However, upon treatment with Cur-AuNPs conjugate, the ROS generating cell population was increased upto 60.00%. This showed that the conjugation has engendered significantly higher ROS in comparison to the individual treatments.

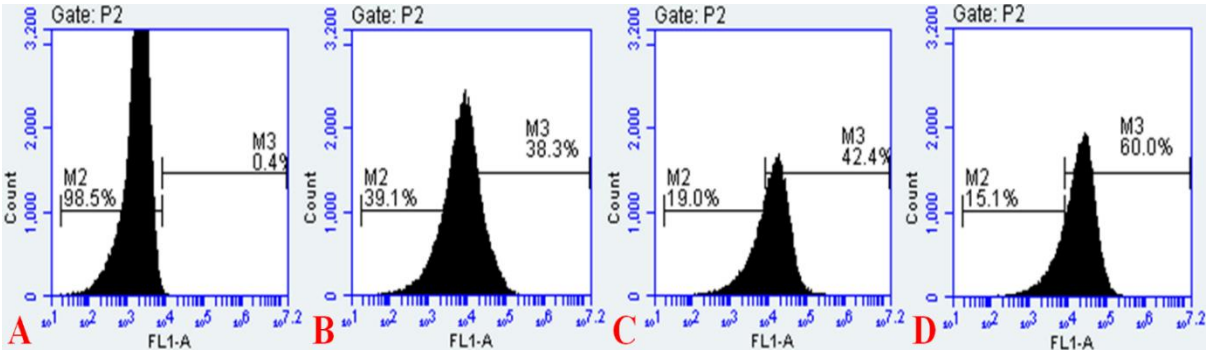

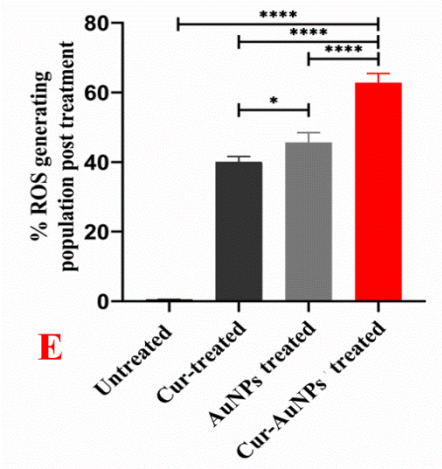

Figure 3.10 *DCFH$_2$DA assay for ROS generation A) Untreated B) Curcumin treated (128 µg/ml) C) AuNPs treated (32 µg/ml) D) Cur-AuNPs treated (8 µg/ml). (Graph was generated and analyzed using GraphPad 8.0 (San Diego, CA) (E) Statistical analysis of ROS generating cell population for untreated, Cur (128 µg/ml) treated, AuNPs (32 µg/ml) treated and Cur-AuNPs (8 µg/ml) treated*

In this article, we reveal that Cur-AuNPs increases the killing potential by increasing membrane permeability and offers avidity for several cellular targets, with intolerable ROS augmentation. We demonstrate that death results from its entrapment along the width of the cell membrane, which denatures the membrane and triggers the production

of ROS. High concentrations of hydroxide free radicals act as a buffer against enzymes that would normally quench ROS. It was hypothesised that this produced ROS causes the release of Fe-S clusters, which would change the iron and energy balance. Under these circumstances, it is conceivable that bacteria's inability to reduce the amount of intracellular ROS result in membrane rupture and, eventually, cell death.

Through the application of phenotypic analyses, we have demonstrated here how the disruption of several bacterial cellular functions by Cur-AuNPs leads to changes in the cell membrane's permeability and the production of excessive ROS in bacterial isolates. Our investigation proposes that the curcumin skeleton's natural thiophilic chemical properties which are now water dispersible are the cause of this multi-targeted antimicrobial mechanism of action. Through mechanistic investigations, we are able to establish that Cur-AuNPs can enhance its effectiveness as an antibacterial agent.

3.2.7 Biocompatibility

The effects of the Cur, AuNPs, and Cur-AuNPs (concentration 128 µg/ml, 32 µg/ml and 8 µg/ml, respectively) used in this research were then investigated for potential toxicity to mammalian systems. For this, we performed an MTT assay on MG-63 cell lines to investigate the in vitro toxicity. Our results indicated that direct contact with synthesized nanoparticles samples seemed to have no adverse effects on the viability of the cells. Figure 3.11 shows the variation in mean optical densities (live cells) of MG-63 cells treated with Cur, AuNPs, Cur-AuNPs and untreated cells. It is clearly seen by statistical analysis that the treated cells exhibited significant difference in mean cell viability than untreated cells. Also, significant (statistical) increase in the cell proliferation is obtained for the cultured cells, incubated for 5 and 7 days with respect to those for 3 days, irrespective of any treatment.

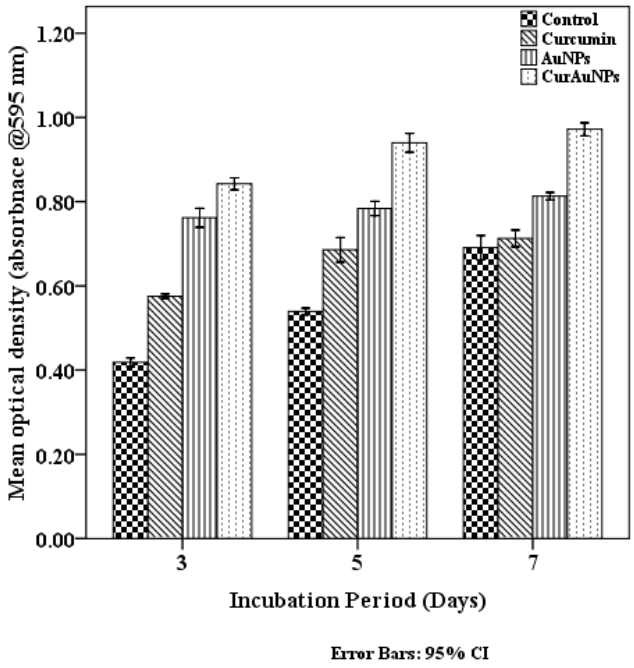

Figure 3.11 *MTT Assay for control and Cur (128 µg/ml), AuNPs (32 µg/ml) and Cur-AuNPs (8 µg/ml) treated MG-63 cell line after 3, 5 and 7 days of incubation.*

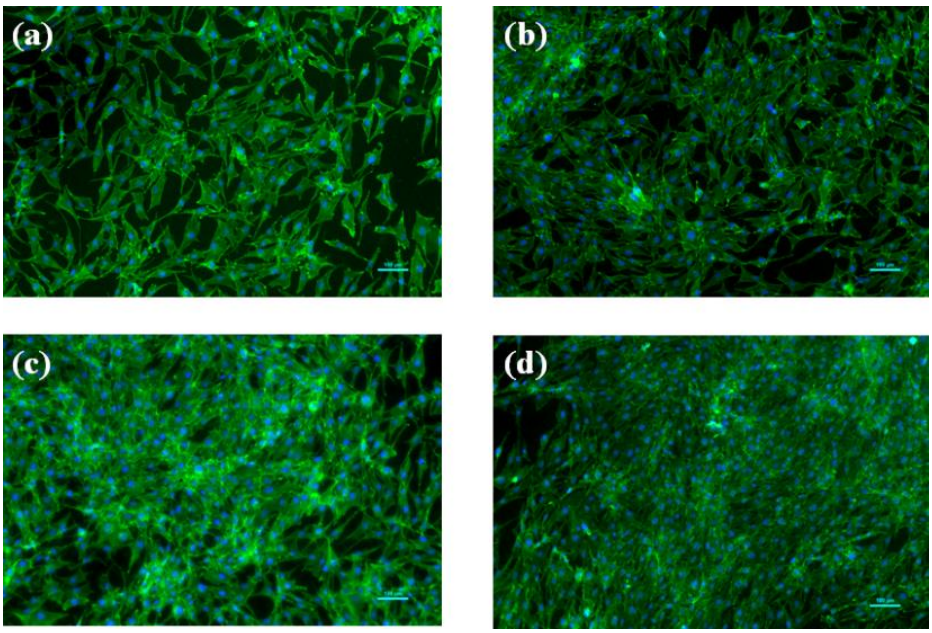

Figure 12 *Fluorescence image of MG-63 cultured for 5 days (a) control, (b) Cur (128 µg/ml) treated, (c) AuNPs (32 µg/ml) treated, (d) Cur-AuNPs (8 µg/ml) treated. (Scale bar 100µm).*

Further, it has been observed that Cur-AuNPs treatment accelerate cell proliferation in contrast to Cur & AuNPs treatment. It can, therefore, be concluded that the curcumin conjugated AuNps significantly increases the cell growth and proliferation as compared to AuNPs alone.

Morphological evaluation of Cur, AuNPs, Cur-AuNPs treated and untreated MG-63 cells via fluorescence microscopy was shown in Figure 3.12. The cell density is observed to be higher in Cur-AuNPs treated cells as compared to Cur and AuNPs treated group. In addition, cells appear to be denser and more flattened in Cur-AuNPs treated cells. Thus, it can be inferred that Cur, and Cur-AuNPs treatment have insignificant toxicity on human cell line.

Future research in the fields of synthetic chemistry for pharmaceutical development and the nano sciences will inevitably explicitly design new alterations in AuNPs surface to generate more robust and comprehensive treatments. We may also consider implementing soluble curcumin-metal complexes that might be employed to encapsulate medical implants that are susceptible to secondary infections. We can also develop a conjugated nanomaterial that, when essential, stimulates a controlled release of these curcumin-conjugates at the infection site.

3.3 Conclusion

In conclusion, we have proposed a simple route to conjugate curcumin with AuNPs which are highly stable in aqueous medium at room temperature. Diarylheptanoid chromophore group of curcumin and plasmon resonance signature of gold remain intact after conjugation ensuring the bio-active nature of curcumin and gold signature. Also, the synthesised Cur-AuNPs showed excellent antibacterial and antibiofilm activity. In addition, we checked the biosafety profile of Cur-AuNPs by cell culture (MG-63 cell

line) to ensure its biocompatibility. The zeta potential on the surface of AuNPs and Cur-AuNPs was more than ±25 mV which is a sign of their high stability. The curcumin conjugated AuNPs were also showed selective synergistic toxicity on bacteria (*Klebsiella pneumonia*) over mammalian cells (MG-63 cell line), and the dramatic decrease in MIC of AuNPs after conjugation with curcumin signals the possible feasibility of systemic medical use of Cur-AuNPs. These activities indicate that the synthesized Cur-AuNPs are possible candidates for use in various biomedical applications.